Available online at www.sciencedirect.com
ScienceDirect
Geotextiles and Geomembranes 25 (2007) 311–323
Geotextiles and Geomembranes
www.elsevier.com/locate/geotexmem

Geosynthetics reinforcement application for tsunami reconstruction: Evaluation of interface parameters with silty sand and weathered clay

P.V. Long[a], D.T. Bergado[b,*], H.M. Abuel-Naga[c]

[a] Vina Mekong Engineering. Consultants, Ho Chi Minh City, Vietnam
[b] School of Engineering and Technology, Asian Institute of Technology, PO Box 4, Klong Luang, Pathumthani 12120, Thailand
[c] Department of Civil Engineering, Monash University, Melbourne, Vic. 3800, Australia

Accepted 2 February 2007
Available online 20 April 2007

Abstract

Great attention is directed to rebuild livelihoods and rehabilitate coastal communities affected by the Tsunami in the Indian Ocean in South Asia. It takes years of effort of different engineering disciplines to recover from recent devastations caused by the Tsunami. Geosynthetics can play important and vital roles in the protection, mitigation and rehabilitation efforts in affected coastal areas. Geosynthetics can be applied for reinforcement, filtration, drainage, protection, lining, and containment. Particularly, geotextiles can be used effectively for erosion protection and for reinforcement of earth embankments to resist failure during the occurrence of earthquakes associated with tsunami. Presented in this paper is the interaction behavior at pullout interfaces of high strength geotextile confined in weathered clay and silty sand. The interface parameters which are needed for both finite element and conventional analyses of geotextile-reinforced earth structures such as the local shear stress/shear displacement, the interface interaction coefficient and the in-soil stress/strain of the reinforcement have been successfully interpreted by the newly proposed method considering the softening behavior and non-uniform distribution of shear stress along the extensible reinforcement. Results from this study indicate that the interpretation of pullout tests using conventional methods underestimated both the shear stiffness and the peak shear strength at the pullout interface of extensible reinforcement.

Keywords: Tsunami; Geotextile reinforcement; Weathered clay; Silty sand; Interaction parameter; Pullout test

1. Introduction

The Asian Tsunami of 26 December 2004, which struck the Indian Ocean Basin, affected hundreds of thousands of people in countries including Thailand, Sri Lanka, Indonesia and India. Its death toll has risen to over 260,000 victims. Many survivors had their lives disrupted since coastal tourism, fisheries, and agriculture have been seriously affected. Housing and public infrastructures have been destroyed Warnitchai (2005). There is urgent need to restore, rehabilitate and repair the damages of the affected people and the area.

Geosynthetics can play important and vital roles in the protection, mitigation and rehabilitation efforts in affected coastal areas. Geosynthetics have been used in hydraulic and geotechnical engineering for about the past two or three decades. Their use is well established for the purposes of material separation, filters (Faure et al., 2006; Liu and Chu, 2006; Muthukumaran and Ilamparuthi, 2006; Wu et al., 2006), and reinforcement (e.g. Bathurst et al., 2005; Kazimierowicz-Frankowska, 2005; Park and Tan, 2005; Skinner and Rowe, 2005; Varsuo et al., 2005; Al Hattamleh and Muhunthan, 2006; Hufenus et al., 2006; Nouri et al., 2006).

In addition, all kinds of bags are made now from synthetic fabric. The functions and geosynthetic types are tabulated in Table 1. The use of geosynthetics has advantages such as speed of construction, flexibility and durability, use of local soil materials rather than imported

*Corresponding author. Tel.: +66 2 524 5512; fax: +66 2 524 6050.
E-mail addresses: h2pvl@vnn.vn (P.V. Long), bergado@ait.ac.th (D.T. Bergado), hossam.abu-elnaga@eng.monash.edu.au (H.M. Abuel-Naga).

0266-1144/$ - see front matter © 2007 Elsevier Ltd. All rights reserved.
doi:10.1016/j.geotexmem.2007.02.007

Table 1
Function versus geosynthetic type

Type of geosynthetics	Separation	Reinforcement	Filtration	Drainage	Containment
Geotextile	√	√	√	√	
Geogrid		√			
Geonet				√	
Geomembrane					√
Geosynthetic clay liners					√
Geopipes				√	
Geofoam	√				
Geocomposites	√	√	√	√	√

quarry product, and its cost effectiveness. Therefore, it is strongly recommended to use the geosynthetics engineering applications for restoring and rehabilitation of the recent devastations caused by the Tsunami. This paper demonstrates the geosynthetic applications of high-strength geotextile to mitigate tsunami devastations focusing on soil reinforcement application.

The use of geosynthetics has unique advantages over other soil strengthening techniques, due to their low mass per unit area, strength, and stiffness characteristics. However, the use of geosynthetics requires a proper understanding of soil–geosynthetic interaction mechanisms. The pullout behavior of geogrids and geotextiles has been investigated by full-scale tests, laboratory model tests and numerical analyses (Jewell et al., 1985; Mitchell and Villet, 1987; Cowell and Sprague, 1993; Lopes and Ladeira, 1997; Ochiai et al., 1996; Khera et al., 1997; Koutsourais et al., 1998; Tatlisoz et al., 1998; Goodhue et al., 2001; Sugimoto and Alagiyawanna, 2003; Desai and El-Hoseiny, 2005; Moraci and Recalcati, 2006; Moraci and Gioffrè, 2006). However, most of the previous studies were directed to investigate the interaction parameters (i.e., pullout resistance and shear stress–strain characteristics) between geosynthetics and granular soils. Few researches have been done relevant to the evaluation of the interaction parameters between the cohesive soils and the geosynthetics (Collin, 1986; Bergado et al., 1991; Keller, 1995; Almohd et al., 2006). Utilizing of cohesive soils would involve considerable savings on condition that the intended engineering purpose can be achieved. In this paper, the interactions of high-strength geotextile with silty sand and weathered clay have been compared.

In the following, the Tsunami devastation effects in Thailand are presented briefly. Then, proposals for mitigation and rehabilitation of coastal areas using geosynthetics engineering are discussed. After that, a newly proposed method for properly interpreting the pullout behavior of extensible reinforcements is described. Then, the interaction behavior, which was interpreted from large pullout tests of high-strength geotextile reinforcement confined in both silty sand and weathered clay, are presented and discussed.

2. Tsunami and devastations in Thailand

The Tsunami wave height distributions in Thailand are shown in Fig. 1. The wave heights were greater at flat shorelines and shallow seawater depths. Consequently, beach resorts with deeper seawater depths and steeper shorelines only experienced slight damages (Warnitchai, 2005). In the aftermath of the large-scale disaster, destructions related to coastal areas and waterways as well as infrastructures and buildings have been identified. Fig. 2 shows the airphoto before and after tsunami at Khao Lak, Phanga, Thailand. The erosion and scouring in the coastlines and waterways can be observed. More details of coastal erosion at Khao Lak are shown in Fig. 3. Small and weak buildings directly open to the coastline were completely destroyed while large and strong buildings remain standing. The foundations of buildings are damaged by scouring and erosion. Erosion damage also occurs on seawalls and earth structures.

Ground elevation is a key factor. Even a small hill of 2 m height has saved houses on it. In fact, the natural sand dune deposits at Karon Beach in Phuket, Thailand, has reduced the destructive effects of Tsunami. There were selective damages of the beaches in Phuket depending on the morphology, topography and depth of seawater of the coastal areas.

3. Proposals for mitigation and rehabilitation of coastal areas

Abednego (2005) presented the proposals by the Indonesian Engineering Association (IEA) for the construction of buffer zone and canal (Fig. 4) as well as "escape mountain" and buildings (Fig. 5). The buffer zone serves to dissipate the impact of strong waves generated by Tsunami. Consequently, the buffer zones are located close to the seashore. These zones may consist of natural barrier such as mangrove forest. Man-made high road embankments and artificial elevated sand dunes can also function as buffer zones. The road embankments should have at least 2.0 m high and 6.0 m wide that can also function as coastal road. The road embankment should be reinforced and erosion resistant through the incorporation of

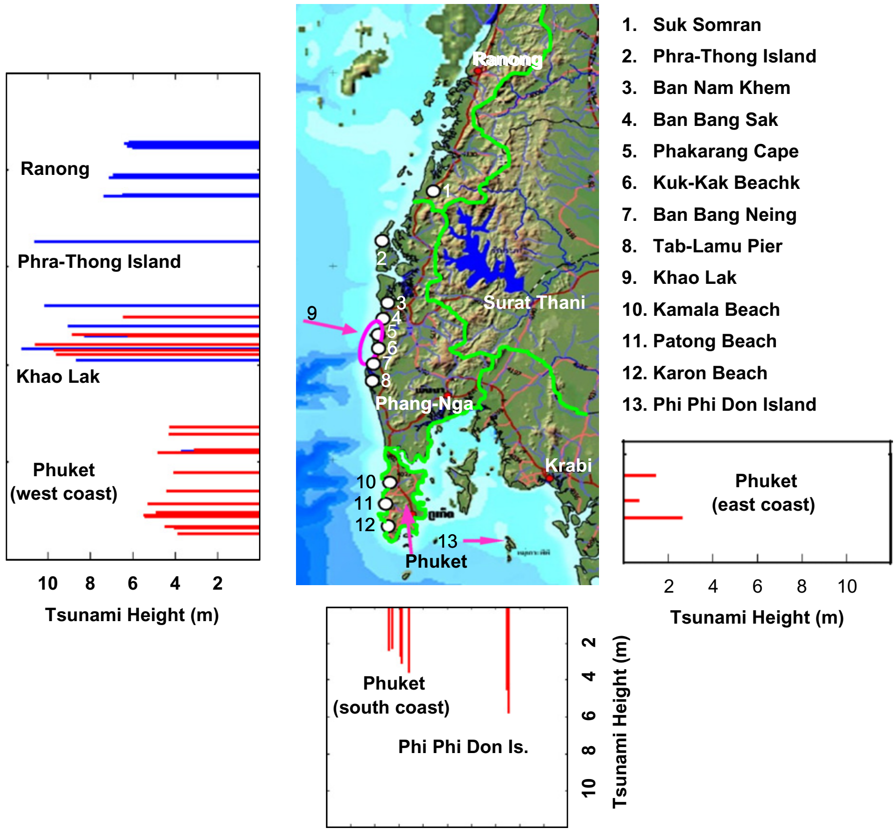

Fig. 1. Tsunami waveheight distribution in Thailand (Warnitchai, 2005).

Fig. 2. Coastal erosion due to tsunami in Khao Lak, Phanga, Thailand (IKONOS Image, Space Imaging/CRISP-Singapore).

geosynthetics (Fig. 6). The artificial sand dunes can be constructed using geotubes or geobags, which are also made of geosynthetics.

Geosynthetic can be also incorporated in the design of the "escape mountain". The escape mountain or hill is constructed similar to a pyramid with geosynthetic reinforcements and erosion protection. The escape mountain or hill can be from 3.0 to 5.0 m high with 30.0 m × 15.0 m rectangular area at the top in order to accommodate at least 1800 people. Unlike the escape tower, the escape mountain or hill allows the access of people in all four sides (Fig. 7). As mentioned earlier, the reinforcement application of geosynthetic material is the focus of this paper. In the following sections, a newly proposed method for properly interpreting the pullout behavior of extensible reinforcements is described. Then, the interaction behavior, which was interpreted from large pullout tests of high-strength geotextile reinforcement confined in both silty sand and weathered clay, are presented and discussed.

4. Reinforcement in pullout test

As mentioned earlier, the pullout mechanism of reinforcements from soils has been commonly investigated by pullout tests. However, at present, pullout tests on geotextile reinforcement have not been interpreted satisfactorily. The high elongation, confinement-dependent behavior of geosynthetics, and the slippage at the clamped end during pullout are still the main barriers for obtaining reliable results. The commonly used method (Collios et al., 1980; Mitchell and Villet, 1987) for interpretation of pullout tests were based on the assumption of uniform distribution of stress, and thus, the pullout shear stress was obtained as follows:

$$\tau = P/2L = \sigma \tan \delta_a + c_a, \quad (1)$$

Fig. 3. Coastal erosion due to tsunami in Khao Lak, Phanga, Thailand.

where P is the pullout force per unit width of reinforcement, σ is total normal stress at interface, δ_a and c_a is friction angle and cohesion at pullout interface, respectively, L is displaced length of the reinforcement corresponding to pullout force, P.

The values of the displaced length (effective length), L, can be obtained from the measured displacements at various points inside the shear box (Hayashi et al., 1994). However, the assumption of uniform distribution of shear stress along the soil–reinforcement in pullout loading is not reliable for the case of extensible reinforcement (Mitachi et al., 1992; Bourdeau et al., 1994; Long et al., 1995). A general distribution of reinforcement displacement, $u(x)$, shear stress distribution at interface, $\tau(x)$, and tension force (per unit width), $T(x)$, along the reinforcement can be schematically illustrated in Fig. 8. The relation between shear stress, τ, acting along an infinitesimal interface, $\mathrm{d}x$, and the mobilized tensile force per unit width of the reinforcement, T, is expressed by the following equation:

$$\frac{\mathrm{d}T}{\mathrm{d}x} = 2\tau. \tag{2}$$

The shear stress given by Eq. (2) is the "local" shear stress at a considered point while the shear stress presented in Eq. (1) is the "global" shear stress along the displaced length. As can be seen in Fig. 1b and c, the shear stress interpreted by Eq. (1), referred to as the conventional method, is generally smaller than those calculated from Eq. (2).

5. Method of interpretation

The compatibility between displacement, u, and tensile strain, E, of the reinforcement is given as follows:

$$\frac{\mathrm{d}u}{\mathrm{d}x} = \varepsilon. \tag{3}$$

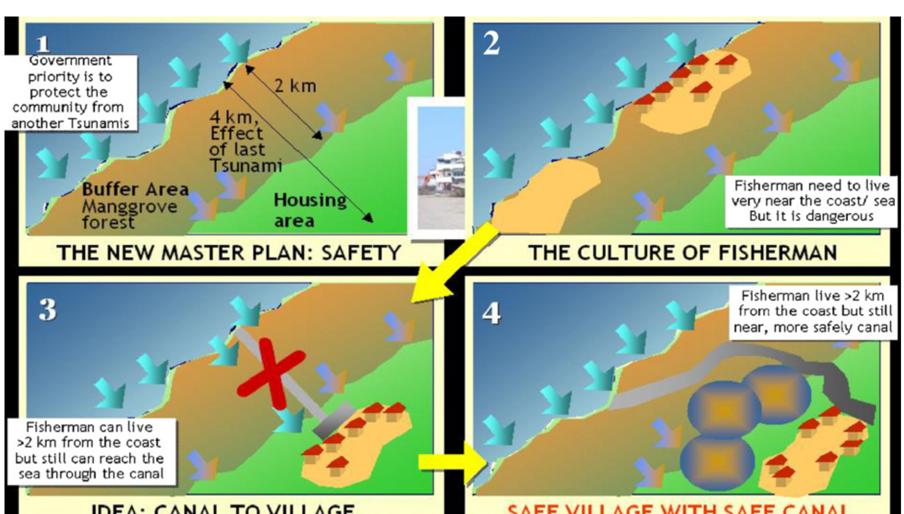

Fig. 4. Proposal for buffer zone and channel (Abednego, 2005).

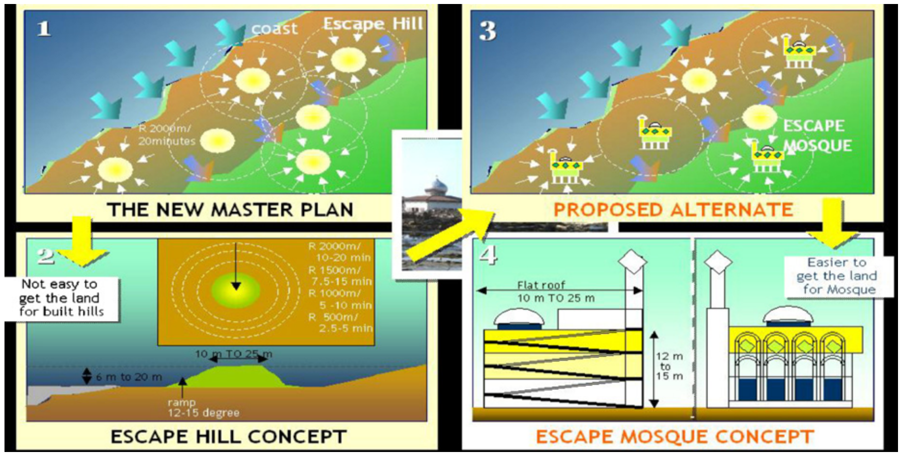

Fig. 5. Proposal for escape building or hill (Abednego, 2005).

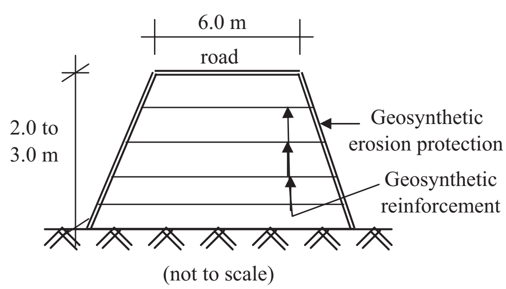

Fig. 6. Reinforced high road embankment in buffer zone.

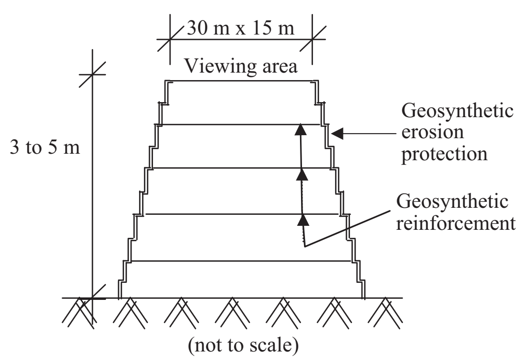

Fig. 7. Escape mountain concept.

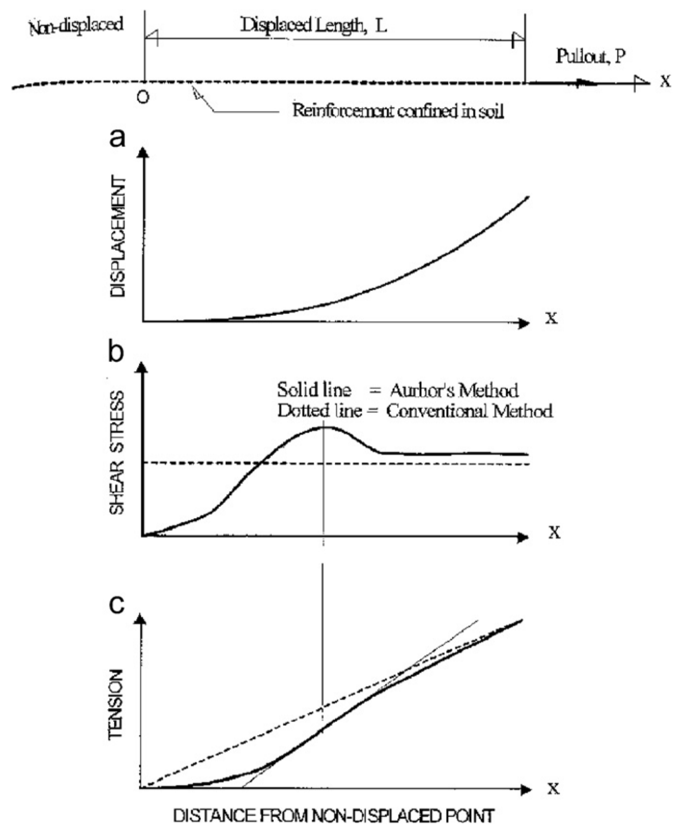

Fig. 8. Schematic diagrams for distribution of displacement, shear stress, and tension along the extensible reinforcement in pullout test.

The tangent stiffness of the in-soil tension-strain of reinforcement, S_t can be expressed as

$$S_t = \frac{dT}{d\varepsilon}. \tag{4}$$

Differentiation of Eq. (3) and substitution for T and E from Eqs. (2) and (4), the governing equation at soil–geotextile interface can be obtained as follows:

$$\frac{d^2u}{dx^2} = \frac{2\tau}{S_t}. \tag{5}$$

Under the pullout force per unit width of reinforcement, P, the reinforcement displacements are assumed to decrease gradually from the pullout end to some location having, no displacement (non-displaced point) as given in Fig. 8. Thus, the reinforcement displacement, $u = y(x)$, is an ascending, non-linear function of x as presented in Fig. 9. Practically, the plot of $y(x)$ can be divided into small segments so that in each segment, the function $y(x)$ can be

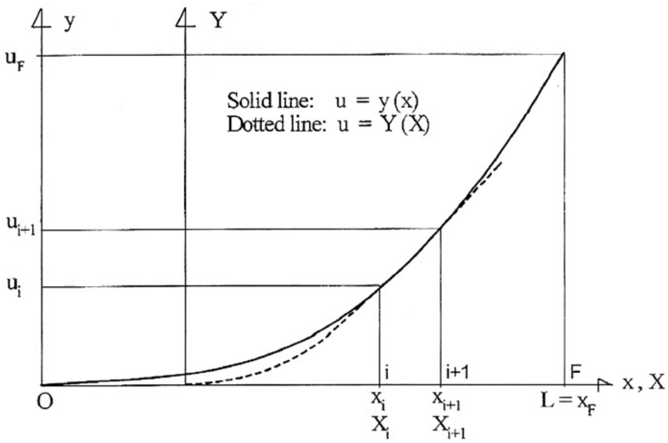

Fig. 9. Approximation for the distribution of reinforcement displacements.

approximated by a parabola, $Y(X) = AX^2$, in local coordinate (X, Y) as illustrated in Fig. 9. Thus, under the pullout P_j, for the segment i from node i to node $i+1$, the approximated displacement can be written in the following form:

$$u_{i,j} = y_j(x) \approx Y_{i,j}(X) = A_{i,j}X^2 \quad \text{for} \quad X_{i,j} \leqslant X \leqslant X_{i+1,j} = X_{i,j} + \Delta x. \tag{6}$$

The physical meaning of the curve-fitting coefficient, A_{ij} can be obtained from Eqs. (5) and (6) as follows:

$$A_{i,j} = \tau_{i,j}/S_{i,j}. \tag{7}$$

Rewriting Eq. (6) for nodes i and $i+1$:

$$u_{i,j} = A_{i,j}X^2_{i,j}, \tag{8a}$$

$$u_{i+1j} = A_{i,j}X^2_{i+1j}. \tag{8b}$$

Eqs. (8a) and (8b) lead to:

$$\sqrt{A_{i,j}} = \frac{\sqrt{u_{i+1,j}} - \sqrt{u_{i,j}}}{\Delta x}, \tag{9}$$

where

$$\Delta x = x_{i+1,j} - x_{i,j} = X_{i+1,j} - X_{i,j}. \tag{10}$$

Therefore, from the measured values of reinforcement displacement at two adjacent locations i and $i+1$ under various values of pullout, P_j, the values of A_{ij} can be computed. Then, from the ($A_{i,j}$ versus $u_{i,j}$) plot, the function $A = f(u)$ can be established for the general relation between the displacement, u, and the corresponding coefficient A.

6. Pullout displacement

The pullout displacement is usually measured at the pullout head outside the shear box. This displacement includes the unavoidable slippage between the reinforcement and the clamping system as well as the deformation of the connection system from the inner clamps to the measured location. Therefore, the following extrapolation scheme has been derived for obtaining the pullout displacement excluding the aforementioned effects.

Eq. (8b) can be written in the other form as

$$u_{i+1,j} = A_{i,j}(X_{i,j} + \Delta x)^2 = u_{i,j} + A_{i,j}\Delta x^2 + 2A_{i,j}X_i\Delta x. \tag{11}$$

From Eqs. (3) and (6), the reinforcement strain, $\varepsilon_{i,j}$, at node i can be expressed by

$$\varepsilon_{i,j} = \mathrm{d}u/\mathrm{d}X = 2A_{i,j}X_i. \tag{12}$$

Eqs. (11) and (12) yield

$$u_{i+1,j} = u_{i,j} + A_{i,j}\Delta x^2 + \varepsilon_{i,j}\Delta x. \tag{13}$$

For any integer value k, Eq. (13) can be written for the general case of node $i+k-1$ as follows:

$$u_{i+k+1,j} = u_{i,j} + A_{i+k,j}\Delta x^2 + \varepsilon_{i+k,j}\Delta x. \tag{14}$$

The strain $\varepsilon_{i+k,j}$ in Eq. (14) can be calculated from the nodal displacements of the segment $(i+k+1)$ as follows:

$$\varepsilon_{i+k,j} = (u_{i+k,j} - u_{i+k-1},j))/\Delta x + A_{i+k-1,j}\Delta x. \tag{15}$$

Suppose that the reinforcement portion from node $i+1$ to the pullout end at node F, is divided into n segments having equal intervals, Δx, the displacement at pullout end, $u_{Fj} = u_{i+1+n,j}$, can be calculated by Eqs. (14) and (15) for $k = 1$ to n from the known values of $u_{j,j}$ and $u_{j+1,j}$. Then the pullout–displacement relation can be obtained as the plot of P_j versus u_{Fj}.

7. Pullout–displaced length

The ascending function for displacement, $u = y(x)$, yields the following behavior:

$$u_{i+1,j} = u_{i,j+1} \leftrightarrow x_{i+1,j} = x_{i,j+1}. \tag{16}$$

Substitution for $u_{i+1,j}$ and $x_{i+1,j}$ from Eq. (16) into Eqs. (10) and (11), one obtains:

$$\sqrt{A_{i,j}} = \frac{\sqrt{u_{i+1,j}} - \sqrt{u_{i,j}}}{x_{i,j+1} - x_{i,j}}. \tag{17}$$

Eq. (17) is also true for any value of j satisfying the increment of $(x_{i,j+1} - x_{i,j}) \leqslant \Delta x$. Rewriting Eq. (17) for node F at the pullout end, the increment of displaced length, $\Delta L_j = x_{\mathrm{F}j+1} - x_{\mathrm{F}j} \leqslant \Delta x$, that was caused by the incremental pullout, $\Delta P_j = P_{j+1} - P_j$ can be obtained in the following form:

$$\Delta L_j = \frac{\sqrt{u_{F,j+1}} - \sqrt{u_{F,j}}}{\sqrt{A_{F,j}}}. \tag{18a}$$

Then, the displaced length, L_{j+1}, corresponding to the pullout force, P_{j+1}, can be calculated as the sum of displaced–length increments as follows:

$$L_{j+1} = \sum_{0}^{j} \Delta L_j. \tag{18b}$$

From Eq. (2), it can be derived that the slope of pullout–displaced length curve is twice of the shear stress at

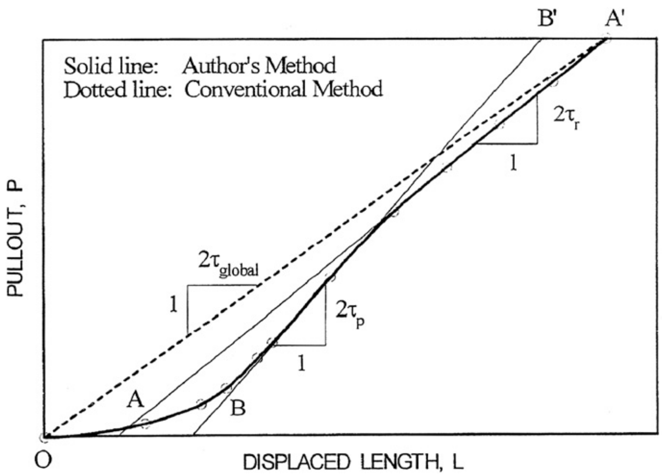

Fig. 10. Interpretation of shear strength at soil–reinforcement interface.

interface. Therefore, the shear strength parameters at interface can be determined directly from the (P_j versus L_j) plot in the manner of Fig. 10. The peak shear strength, τ_p, and the critical state strength, τ_r, at pullout interface can be obtained from the slopes of lines BB′ and AA′, respectively, as seen in Fig. 10.

8. Shear stress–relative shear displacement at interface

From Eq. (2), the shear stress, τ_j, corresponding to the pullout displacement u_{Fj} can be expressed by the following equation:

$$\tau_{Fj} = \frac{T_{F,j+1} - T_{F,j}}{2\Delta L_j} = \frac{P_{j+1} - P_j}{2\Delta L_j}, \tag{19}$$

where $T_{F,j+1}$ and $T_{F,j}$ are tension forces per unit width of the reinforcement at the pullout end that are equal to the pullout P_{j+1} and P_j, respectively.

9. Reinforcement strain

From Eqs. (15) and (16), the in-soil strain of the reinforcement, $\varepsilon_{F,j+i}$, corresponding to the tension at the pullout end, $T_{F,j+1} = P_{j+i}$, can be derived as follows:

$$\varepsilon_{F,j+1} = (u_{F,j+1} - u_{F,j})/\Delta L_j + A_{F,j}\Delta L_j. \tag{20}$$

Thus, the in-soil tension/strain relation can be constructed from the P_j versus $\varepsilon_{F,j}$ plot.

10. Summary of interpretation procedures

As presented in the previous sections, only two measured locations of reinforcement displacement are needed for interpretation of the behavior at pullout interface including the in soil tensile stress–strain of the reinforcement. Assume that the displacements are measured at points B and C in Fig. 11. To satisfy the assumption of parabolic distribution of displacement within the considered segment, the distance between these measured points should be selected based on the stiffness of the reinforcement. If length FB and BC is not the same, the value of Δx must be taken as the actual interval of the corresponding points. For convenience, the value of $i = 1$ can be assigned for point C. The procedures of interpretation are summarized in the following steps:

Step 1: Using Eq. (9) and $\Delta x = \text{CB}$ to calculate the coefficient $A_{i,j}$ from the measured displacement at C and B, denoted as u_{1j} and u_{2j}, respectively. Construct the (A_{1j} versus u_{1j} plot and obtain the general relation $A = f(u)$ from this plot, e.g. by curve fitting.

Step 2: Calculate ε_{2j} by Eq. (15) using $k = 1$ and $\Delta x = \text{BC}$. Compute $A_{2j} = f(u_{2j})$ for segment CF, then obtain the displacement at the pullout end, $u_{Fj} = u_{3j}$, using $\Delta x = \text{CF}$ in Eq. 14. The pullout–displacement relation can be plotted from the values of P_j and u_{Fj}.

Step 3: Calculate A_{Fj} from the values of u_{Fj}. Then, the relations of pullout–displaced length, shear stress–shear displacement, and in-soil stress–strain of the reinforcement can be calculated by Eqs. (18b)–(20), respectively. The global strength, τ_{global}, the critical state strength, τ_r, and the peak strength, τ_p, of soil–reinforcement interface can also be determined directly from the pullout–displaced length curves by means of the slopes of the corresponding line OA′, AA′ and BB′, respectively, as illustrated in Fig. 10.

11. Large pullout tests

The high-strength, woven–nonwoven polyester geotextile PEC200 with nominal mass of 700 g/m^2 and rupture strength of 200 kN/m, was used as the reinforcement. The investigation involves the use of weathered Bangkok clay and silty sand (locally known as Ayudthaya sand), which are used widely as fill material for road construction in the Central Plain of Thailand where Bangkok is located. The weathered clay specimen was compacted at 28% water content at a dry density of 15.1 kN/m^3, corresponding to 95% standard Proctor compaction on the wet side of optimum. Likewise, a water content of 13% and dry density of 17.0% kN/m^3, corresponding to about 95% standard Proctor compaction, were maintained for the silty sand samples. The pullout box was made of 9.5 mm thick steel plates with inside dimensions of 1270 mm in length × 762 mm in width × 508 mm in height. The normal stress was applied by a pressurized air bag. The pullout force was applied by a 225 kN capacity electro-hydraulic controlled jack and was measured by an electrical load cell. The clamped end of geotextile was located inside the compacted soil in order to ensure that the geotextile specimen is always confined throughout the pullout test. This way, no coupling of unconfined and confined behavior of geotextile would result during the pullout test, which is an important consideration for extensible reinforcements. The pullout end of geotextile specimen is positioned at 0.25 m from the front wall for minimizing the effects of stress concentration resulted from the reaction of the front wall. The layout of geotextile specimen together with the

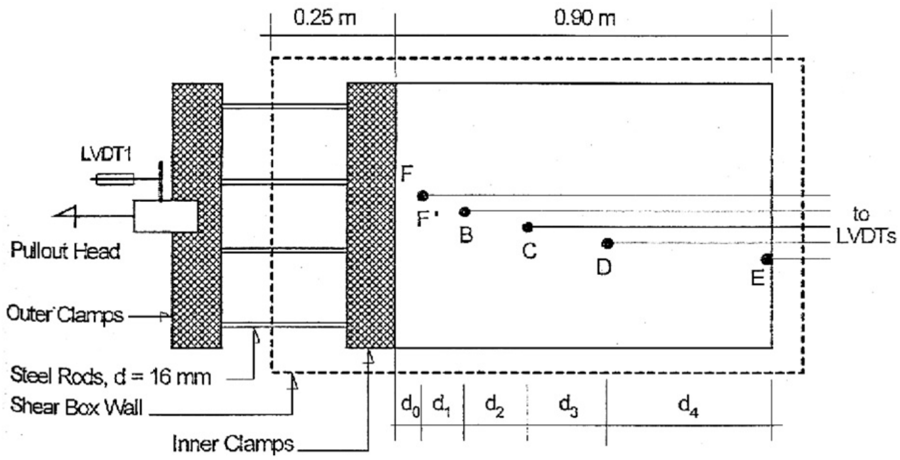

Fig. 11. Clamp system and instrumentation for large pullout test.

clamping system is presented in Fig. 11. The displacements were measured by LVDTs connected to automatic data acquisition (ADA) system. The locations of displacement measurement are also given in Fig. 11. A total of five LVDTs were used. One was attached directly to the outer clamps (pullout head) for measuring the pullout displacement. The other four were connected to the geotextile reinforcement using wire extensometers. The net dimensions of the geotextile specimen were 500 mm in width × 900 mm in length. The pullout rate of 1 mm/min was used for all tests. Four series of pullout tests at different normal stresses of 25, 75 and 125 kPa were performed. To evaluate the resistance contributed by the inner clamping system, two series of dummy tests were also carried out in the same conditions with the corresponding pullout tests but without reinforcements. The net pullout force was obtained as the difference between the pullout test and the corresponding dummy test. Thus, the term "pullout", P, presented in this study is the net pullout force per unit width of reinforcement.

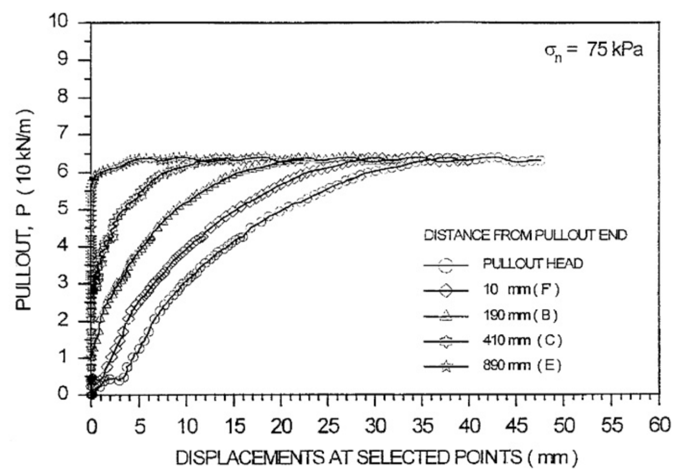

Fig. 12. Pullout–displacement at selected points in pullout test of PEC200/Clay (normal stress = 7.5 tsm).

12. Interpreted results

12.1. Pullout–displacement

The measured pullout–displacements curves at selected points along the reinforcement are plotted in Fig. 12. It can be seen from these figures that the displacement of geotextile reinforcement developed progressively with the increases of pullout force. Using the measured displacements at points B and C (Fig. 12), the curve fitting coefficients, A, were calculated and are presented in Fig. 13 as function of geotextile displacement u. It is interesting to note that the shear stress–shear displacement relations can be roughly estimated from this plot without using the measured pullout force because the value of A is the ratio of shear stress to the reinforcement stiffness, $A = \tau/S$. The stiffness of geotextile PEC200 is almost constant as seen in

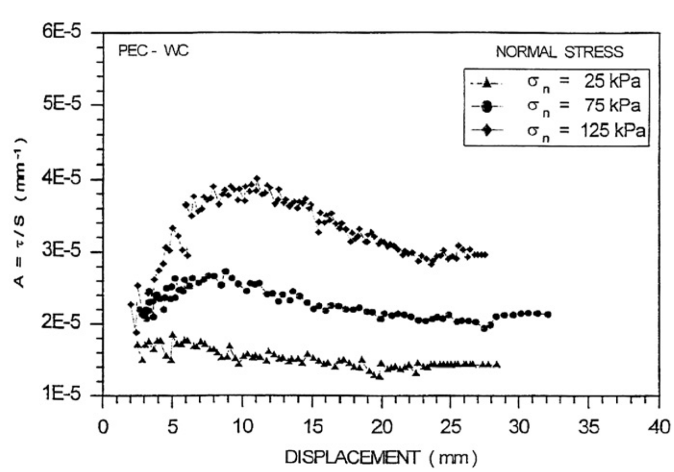

Fig. 13. A versus u relation from pullout tests of PEC200/weathered Clay.

later sections. In other words, the normalized shear stress–shear displacement relation can be approximated in terms of Fig. 13 if the reinforcement stiffness is constant.

The measured displacements along the geotextile at different pullout load levels are presented in Fig. 14. Taking the reference origin at the non-displaced point, these measured displacements fit very well with the calculated relation of displacement, u, versus displaced length, L, presented as the solid line in Fig. 15. The values away from this curve (points with circle in Figs. 14 and 15) are the displacements measured at pullout head outside the shear box. The deviations between these points and the solid line can be considered as the extra displacement consisted of the slippage within the clamping zone and other deformations of the connection system from the inner clamps to the pullout head. The interpreted pullout–displacement curves are presented in Fig. 16 which indicated that the pullout displacement for fully mobilizing pullout strength were in order of 20–30 mm. The corresponding relations of pullout–displaced length that are plotted in Fig. 17 showed the same trend as proposed in Fig. 10 implying the softening behavior at pullout interface. Thus, the peak and critical state shear strength of soil–geotextile interface can be obtained from the slopes of these curves by means of Fig. 10, i.e. the slope of AA′ and BB′ are twice of the critical state shear strength, τ_r, and peak shear strength, τ_p, respectively.

12.2. Behavior at soil/geotextile interface

The shear stress–relative shear displacement relations interpreted from the proposed method are plotted in Figs. 18 and 19 for clay and sand backfill, respectively. The corresponding relationships obtained from the conventional method are also given in these figures as dotted lines for comparison. As mentioned previously, the shear stress interpreted from the proposed method is referred as "local stress", $\tau = \mathrm{d}T/(2\mathrm{d}x)$, at a considered point while the shear

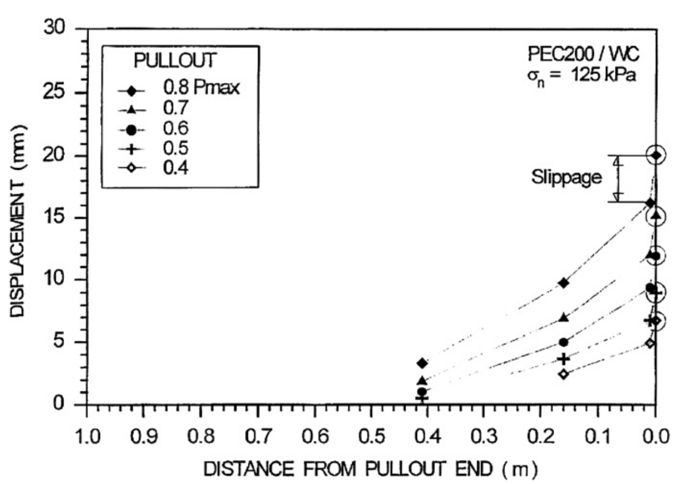

Fig. 14. Typical distribution of Geotextile displacement in pullout test of PEC200/weathered Clay-origin at pullout end.

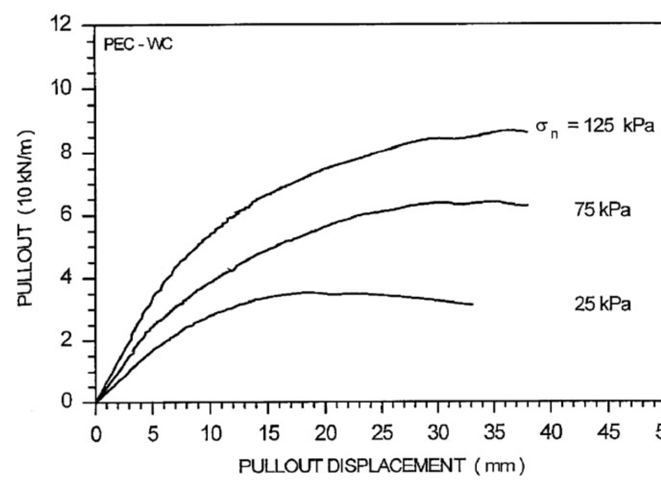

Fig. 16. Pullout–displacement curve for pullout tests of PEC200/weathered Clay.

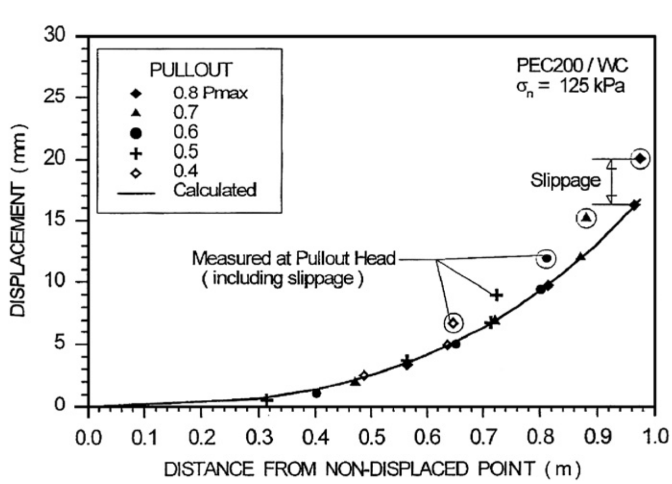

Fig. 15. Measured and calculated Geotextile displacement in pullout test of PEC200/weathered Clay-origin at non-displaced point.

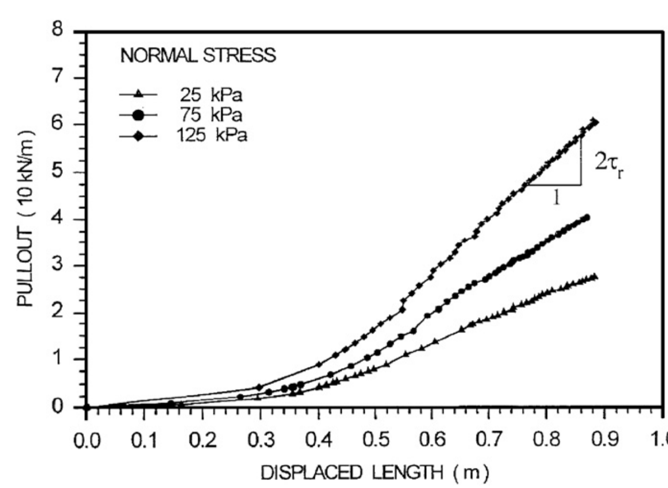

Fig. 17. Pullout–displaced length curves for pullout tests of PEC200/weathered Clay.

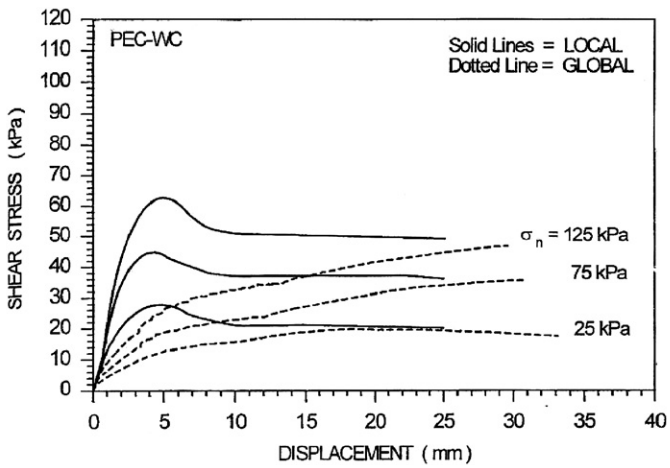

Fig. 18. Shear stress–relative shear displacement curves for pullout interface of PEC200-weathered Clay.

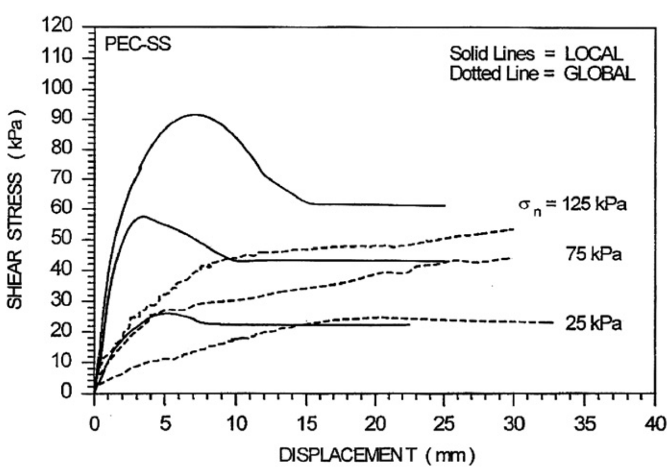

Fig. 19. Shear stress–relative shear displacement curves for pullout interface of PEC200-silty Sand.

stress calculated from the conventional method is the "global stress", $\tau = T/(2L)$, along the displaced length, L. From now on, the terms "global" and "local" are used to refer the interaction behavior interpreted from the conventional method and the author's method, respectively. As seen in Figs. 18 and 19, the local shear stress–relative displacement curves exhibit the softening behavior with peak strength occurring at small relative displacement of about 3–6 mm, while, the global shear stress–pullout displacement gave no distinct peak with displacement as large as 20–30 mm for fully mobilizing shear strength. This is because the displacement of geotextile reinforcement developed progressively along the specimen and, thus, the peak values of shear stress along the soil–geotextile interface cannot be mobilized at the same time. Consequently, the shear stiffness and peak shear strength obtained from the global shear stress were smaller than that interpreted from the local stress. However, when the whole length of the reinforcement had moved under large pullout displacements, both global and local shear stresses were converted to the critical state strength.

The failure envelopes at the soil–geotextile interfaces are plotted in Figs. 20 and 21. The corresponding failure envelopes of soil only by large direct shear tests are also given in these figures as dotted lines for comparison. To evaluate the bonding efficiency at interface, the interaction coefficient, R_i, defined as the ratio of pullout interface shear strength to the soil shear strength determined by the corresponding large direct shear test at the same normal stress, is introduced. It should be noted that the interaction coefficient defined herein can be used very conveniently in modeling the stress–strain relation at soil–reinforcement interface for finite element analysis of reinforced earth structure (Vermeer and Bringkgreve, 1995). The values of R_i calculated from global strength (conventional method) and local strength (author's method) are given in Figs. 22 and 23 for silty sand and weathered clay confinements, respectively. The results indicated that the interaction coefficient is slightly dependent on the normal stress. When

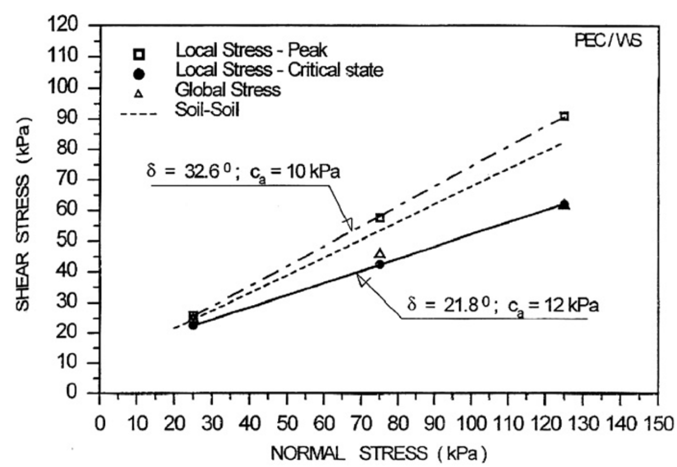

Fig. 20. Failure envelopes for pullout interface of PEC200-silty Sand.

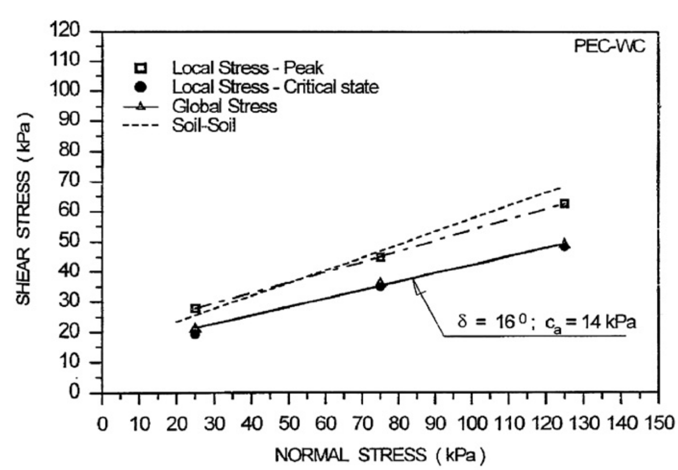

Fig. 21. Failure envelopes for pullout interface of PEC200-weathered Clay.

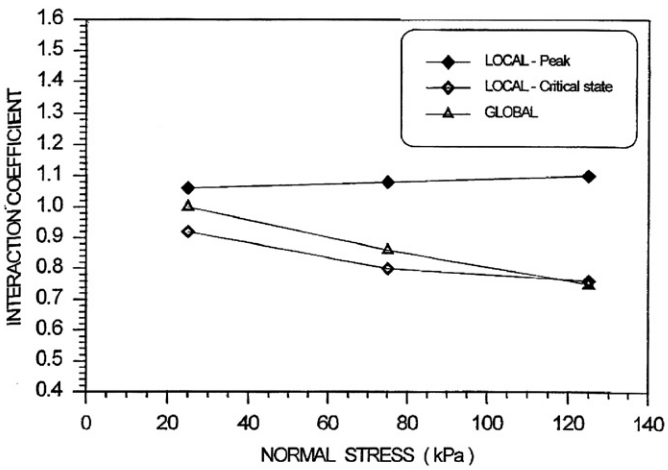

Fig. 22. Interaction coefficients of Sand-PEC200 pullout interfaces.

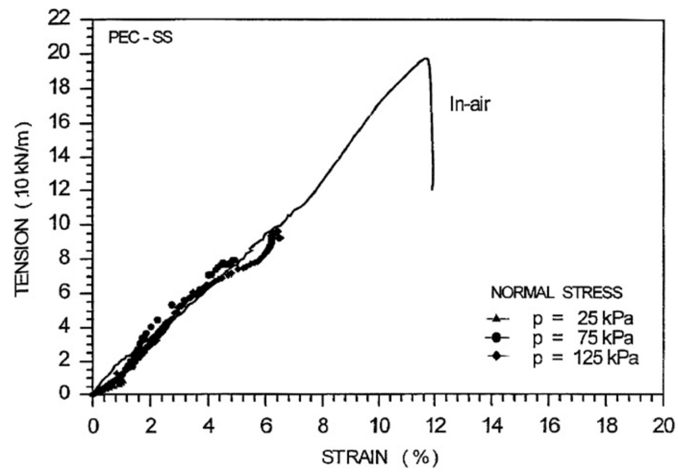

Fig. 24. Tension–strain curves of Geotextile PEC200 with and without confinement of silty Sand.

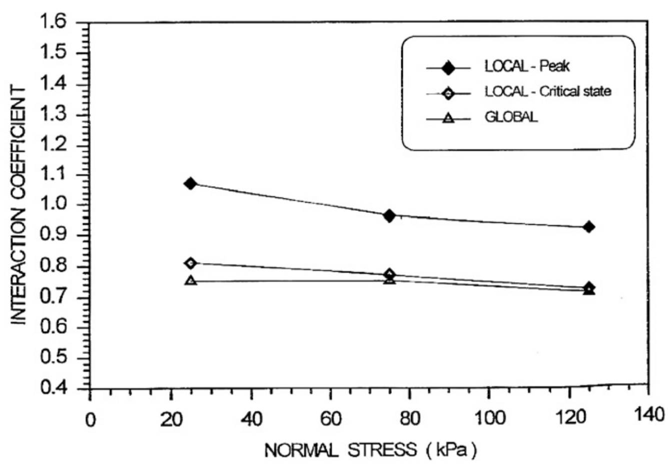

Fig. 23. Interaction coefficients of weathered Clay-PEC200 pullout interfaces.

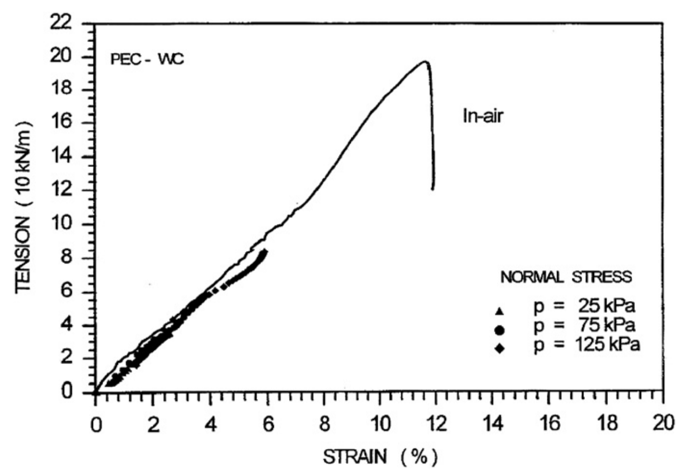

Fig. 25. Tension–strain curves of Geotextile PEC200 with and without confinement of weathered Clay.

normal stress increased from 25 to 125 kPa, the values of R_i calculated by the local strength at critical state decreased from 0.92 to 0.76 and from 0.81 to 0.72 for sand–geotextile and clay–geotextile interfaces, respectively. The corresponding values computed at peak strength are from 1.06 to 1.10 and from 1.07 to 0.92. Moreover, the values of R_i calculated by global strength are almost the same as that computed from local strength at critical state.

13. In soil tension–strain of geotextile

The in-soil, short-term tension–strain relations of geotextile PEC200 interpreted from pullout test results are presented in Figs. 24 and 25 for silty sand and weathered clay confinements, respectively. The in-air tension–strain from a wide-width tensile test (ASTM D-4595) are also presented in these figures as dotted lines for comparison. The results indicated that tensile stress–strain behavior of this geotextile seemed not different in the cases of with and without confinements. This behavior is due to the tension behavior of high-strength geotextile PEC200, which is governed by woven yarns in the main direction. Explanations for the fact that the soil confinement has negligible effects on the stress–strain behavior of woven geotextiles have been given elsewhere (Fock and McGown, 1987).

14. Conclusions

Erosion and scouring resulted from tsunami devastations of coastal areas and waterways. Geosynthetics can be utilized as filters, reinforcements, drainage, containment and separators. Its advantages are lightweight and easy to install with low handling and overall costs. In particular, geotextiles can be utilized effectively for erosion control and earth reinforcement for the construction of "escape mountain or hill" near the coast and earthen berms at buffer zones.

The pullout behavior of high-strength geotextile PEC200 confined in silty sand and weathered clay has been studied by large pullout tests. The measured displacements along the reinforcement implied that the distribution of shear stress along the interface surface was highly non-uniform. Thus, the conventional method of interpretation, which was based on the assumption of uniform distribution of shear stress, would not yield the proper parameters of soil–geotextile interface. A new method considering the softening behavior and non-uniform distribution of shear stress at interface has been presented. The extrapolation scheme for obtaining the net pullout displacement excluding slippage at clamped end has also been included. The method presented herein requires only two locations of displacement measurement in the reinforcement for fully interpreting the soil–geotextile interaction consisting of the shear stress–shear displacement relation and the in-soil tension–strain behavior of the reinforcement. Moreover, the results from this study indicated that the conventional method underestimated both the shear stiffness and the shear strength at the pullout interface.

References

Abednego, L.G., 2005. The contribution of Indonesian Engineers Association to Aceh Province after the Earthquake and Tsunami. Proceedings of the Scientific Forum on Tsunami, its Impact and Recovery, 6–7 June 2005. AIT Conference Center, Bangkok, Thailand.

Al Hattamleh, O., Muhunthan, B., 2006. Numerical procedures for deformation calculations in the reinforced soil walls. Geotextiles and Geomembranes 24 (1), 52–57.

Almohd, I., Abu-Farsakh, M., Khalid, F., 2006. Geosynthetic reinforcement-cohesive soil interface during pullout. In: Hani, H.T. (Ed.), Proceedings of the 13th Great Lakes Geotechnical and Geoenvironmental Conference, Milwaukee, Wisconsin, USA, pp. 40–49.

Bathurst, R.J., Allen, T.M., Walters, D.L., 2005. Reinforcement loads in geosynthetic walls and the case for a new working stress design method. Geotextiles and Geomembranes 23 (4), 287–322.

Bergado, D.T., Shivashankar, R., Sampaco, c.L., Alfaro, M.C., 1991. Behavior of a welded wire wall with poor quality, cohesive-friction backfills on soft Bangkok clay: a case study. Canadian Geotechnical Journal 28, 860–880.

Bourdeau, Y., Ogunro, T., Lareal, P., 1994. Use of strain gages to predict soilgeotextile interaction in pullout tests. Proceedings Fifth Interaction Conference on Geotextiles, Geomembranes and Related Products, vol. 1, 5–9 September 1994, Singapore, pp. 451.

Collin, J.G., 1986. Earth Wall Design. Doctoral Thesis, University of California, Berkeley, California.

Collios, A., Delmas, P., Gourc, J.P., Giroud, J.P., 1980. Experiments on soil reinforcement with geotextiles. Proceedings of the ASCE Symposium on the Use of Geotextiles for Soil Improvement, Portland, p. 53.

Cowell, M.J., Sprague, C.J., 1993. Comparison of pull-out performance of geogrids and geotextiles. Geosynthetics 93, 579–592.

Desai, F.C.S., El-Hoseiny, K.E., 2005. Prediction of field behavior of reinforced soil wall using advanced constitutive model. Journal of Geotechnical and Geoenvironmental Engineering, ASCE 131 (6), 729–739.

Faure, Y.H., Baudoin, A., Pierson, P., Plé, O., 2006. A contribution for predicting geotextile clogging during filtration of suspended solids. Geotextiles and Geomembranes 24 (1), 11–20.

Fock, G., McGown, A., 1987. Creep behavior of a needle punched polypropylene geotextile. Proceedings of the Ninth Southeast Asian Geotechnical Conference, Bangkok, 7–11 December, pp. 101–112.

Goodhue, M.J., Edil, T.B., Benson, C.H., 2001. Interaction of foundry sands with geosynthetics. Journal of Geotechnical and Geoenvironmental Engineering ASCE 127 (4), 353–362.

Hayashi, S., Makuichi, K., Ochiai, H., 1994. Testing methods for soil-geosynthetic friction behavior-Japanese Standard. Proceedings of the Fifth International Conference on Geotextiles, Geomembranes Related Products, vol. 1, Singapore, pp. 411–426.

Hufenus, R., Rueegger, R., Banjac, R., Mayor, P., Springman, S.M., Brönnimann, R., 2006. Full-scale field tests on geosynthetic reinforced unpaved roads on soft subgrade. Geotextiles and Geomembranes 24 (1), 21–37.

Jewell, R.A., Milligan, G.W.E., Sarsby, R.W., Dubois, D., 1985. Interaction between soil and geogrids. Proceedings of the Symposium on Polymer Grid Reinforcement, Civil Engineering, London, pp. 18–29.

Kazimierowicz-Frankowska, K., 2005. A case study of a geosynthetic reinforced wall with wrap-around facing. Geotextiles and Geomembranes 23 (1), 107–115.

Keller, G.R., 1995. Experiences with mechanically stabilized structures and native soil backfill. Transportation Research Record No. 1474, Mechanically Stabilized Backfill and Properties of Geosynthetics and Geocomposites, pp. 30–38.

Khera, R.P., Kasturi, R.M., Khairul Alam, M., 1997. Depth and width effect on pull-out resistance of woven geotextiles in sand. Geosynthetics 97, 851–862.

Koutsourais, M., Sandri, D., Swan, R., 1998. Soil interaction characteristics of geotextiles and geogrids. Geosynthetics 98, 739–744.

Liu, L.F., Chu, C.Y., 2006. Modeling the slurry filtration performance of nonwoven geotextiles. Geotextiles and Geomembranes 24 (5), 325–330.

Long, P.V., Bergado, D.T., Balasubramaniam, A.S., 1995. Interpretation of behavior at pullout interface of soil/geotextile. Proceedings of the 10th Asian Regional Conference on Soil Mechanic and Foundation Engineering, Beijing, China.

Lopes, M.L., Ladeira, M., 1997. Influence of the confinement, soil density and displacement rate on soil–geogrid Interaction. Geotextiles and Geomembranes 14, 543–554.

Mitachi, T., Yamamoto, Y., Muraki, S., 1992. Estimation of in-soil deformation behavior of geogrid under pullout loading. Proceedings of the International Symposium on Earth Reinforcement Practice, Fukuoka/Kyushu, vol. 1, 11–13 November 1992, pp. 121–126.

Mitchell, J.K., Villet, W.C.B., 1987. Reinforcement of earth slopes and embankments, National Cooperative Highway Research Program Report no. 290. Washington, DC, Transportation Research Board, p. 323.

Moraci, N., Gioffrè, D., 2006. A simple method to evaluate the pullout resistance of extruded geogrids embedded in a compacted granular soil. Geotextiles and Geomembranes 24 (2), 116–128.

Moraci, N., Recalcati, P., 2006. Factors affecting the pullout behaviour of extruded geogrids embedded in a compacted granular soil. Geotextiles and Geomembranes 24 (4), 220–242.

Muthukumaran, A.E., Ilamparuthi, K., 2006. Laboratory studies on geotextile filters as used in geotextile tube dewatering. Geotextiles and Geomembranes 24 (4), 210–219.

Nouri, H., Fakher, A., Jones, C.J.F.P., 2006. Development of horizontal slice method for seismic stability analysis of reinforced slopes and walls. Geotextiles and Geomembranes 24 (2), 175–187.

Ochiai, H., Otani, J., Hayashic, S., Hirai, T., 1996. The pull-out resistance of geogrids in reinforced soil. Geotextiles and Geomembranes 14, 19–42.

Park, T., Tan, S.A., 2005. Enhanced performance of reinforced soil walls by the inclusion of short fiber. Geotextiles and Geomembranes 23 (4), 336–348.

Skinner, G.D., Rowe, R.K., 2005. Design and behaviour of a geosynthetic reinforced retaining wall and bridge abutment on a yielding foundation. Geotextiles and Geomembranes 23 (3), 235–260.

Sugimoto, M., Alagiyawanna, A.M.N., 2003. Pullout behavior of geogrid by test and numerical analysis. Journal of Geotechnical and Geoenvironmental Engineering, ASCE 129 (4), 361–371.

Tatlisoz, N., Edil, T.B., Benson, C.H., 1998. Interaction between reinforcing geosynthetics and soil-tire chip mixtures. Journal of Geotechnical and Geoenvironmental Engineering, ASCE 124 (11), 1109–1119.

Varsuo, R.J., Grieshaber, J.B., Nataraj, M.S., 2005. Geosynthetic reinforced levee test section on soft normally consolidated clays. Geotextiles and Geomembranes 23 (4), 362–384.

Vermeer, P.A., Bringkgreve, R.B.J. (Eds.), 1995. Finite Element Code for Soil and Rock Analyses. A.A Balkerma, Rotterdam, Brookfield.

Warnitchai, P., 2005. Lessons learned from the 26 December 2004 Tsunami disaster in Thailand. Proceedings of the Scientific Forum on Tsunami, its Impact and Recovery, 6–7 June 2005 AIT Conference Center, Bangkok, Thailand.

Wu, C.-S., Hong, Y.-S., Yan, Y.-W., Chang, B.-S., 2006. Soil-nonwoven geotextile filtration behavior under contact with drainage materials. Geotextiles and Geomembranes 24 (1), 1–10.